Geometric models for robust encoding of dynamical information into embryonic patterns

Laurent Jutras-Dubé [1], Ezzat El-Sherif [2] *, Paul François [1] *

1 Department of Physics, McGill University, 3600 rue University, H3A 2T8, Montreal, QC, Canada

2 Division of Developmental Biology, Department of Biology, Friedrich-Alexander-Universität Erlangen-Nürnberg, Erlangen 91058, Germany

* Corresponding Authors

Abstract

During development, cells gradually assume specialized fates via changes of transcriptional dynamics, sometimes even within the same developmental stage. For anterior-posterior patterning in metazoans, it has been suggested that the gradual transition from a dynamic genetic regime to a static one is encoded by different transcriptional modules. In that case, the static regime has an essential role in pattern formation in addition to its maintenance function. In this work, we introduce a geometric approach to study such transition. We exhibit two types of genetic regime transitions, respectively arising through local or global bifurcations. We find that the global bifurcation type is more generic, more robust, and better preserves dynamical information. This could parsimoniously explain common features of metazoan segmentation, such as changes of periods leading to waves of gene expressions, "speed/frequency-gradient" dynamics, and changes of wave patterns. Geometric approaches appear as possible alternatives to gene regulatory networks to understand development.

Introduction

28 Development from one zygote to a viable animal is a complex process (Wolpert et al.,

29 2006), comprising multiple dynamical sub-processes, including cell movements, tissue

30 morphogenesis, dynamical gene expressions, and cellular differentiations. Eventually,

31 cell identities are fixed by various mechanisms, such as multistable gene regulatory

32 networks and epigenetic markers. Little is known about how this transition from a

33 dynamic/initiation phase to a static/maintenance one is mediated. Are there general

34 characteristics that should be matched between dynamic and static phases to mediate a

35 robust transition?

36 In dynamical systems theory, transitions between different regimes are called

37 'bifurcations', which are defined as qualitative changes in the dynamics of a system driven

38 by a so-called 'control parameter' (Strogatz, 2015). Bifurcations are of many types but

39 can be systematically classified. For instance, generic families of potentials driving the

40 dynamics have been identified as different "catastrophes" (Poston & Stewart, 2012).

41 While such mathematical descriptions are highly technical, they are reminiscent of the

42 theory of epigenetic landscapes pushed forward by Waddington (Waddington, 1957). It

43 is thus natural to ask if such classifications can be done for development. Could dynamical

44 systems theory help us in this pursuit, and in studying development in general? The main

45 issue here is to frame the problem in a way that allows to derive general results.

46 In recent years, numerous experimental studies have revealed that quantitative changes

47 of gene expressions during development often followed standard predictions from

48 dynamical systems theory (Huang et al., 2007). The Waddington landscape's analogy

49   (Jaeger & Monk, 2014) has led to many insights in cell differentiation (Graf & Enver, 2009),

50   and recent data on cell reprogramming quantitatively validated the associated "landscape

51   picture" (Pusuluri et al., 2018). Geometric models of development have been developed

52   in particular cases, precisely predicting the general phenotypes of wildtype and mutants

53   (e.g. the development of *C. elegans* vulva (Corson & Siggia, 2012) and *Drosophila* brittle

54   patterns (Corson et al., 2017)).

55   The Clock-and-Wavefront model (Cooke & Zeeman, 1976), accounting for the observed

56   dynamical somite (vertebrae precursors) formation, was inspired by catastrophe theory.

57   The model predicted that a retracting wavefront translates the periodic expression of a

58   genetic clock into a spatial pattern via "catastrophic" transitions demarcating the positions

59   of the somites (Figure 1A). Identification of the predicted clock in 1997 (Palmeirim et al.,

60   1997) has since led to many subsequent theoretical and experimental works, including

61   observation of similar clocks in multiple arthropods (El-Sherif et al., 2012; Sarrazin et al.,

62   2012). Cooke and Zeeman originally assumed that the clock is an external process, blind

63   to the subsequent segmentation process it directs (Cooke & Zeeman, 1976). However, it

64   has been very clear from the early experiments in (Palmeirim et al., 1997) that cellular

65   oscillators increase their period prior to segmentation, leading to traveling waves of

66   various signalling pathways such as Notch (Giudicelli et al., 2007; Morelli et al., 2009)

67   (Figure 1A). Importantly, Notch waves eventually stabilize into a pattern of *delta* ligand

68   stripes (Giudicelli & Lewis, 2004; Jiang et al., 2000), with a functional continuity between

69   the dynamic and the static regime. Indeed, it has been shown that the dynamical phase

70   of the clock is encoded into static rostro-caudal identities (Oginuma et al., 2010). This

71   suggests that the observed oscillation is not a simple external pacemaker for segment

72 formation: rather, clocks, associated waves and eventual stripe formations combine into

73 an emergent process leading to proper fate encoding. Segmentation thus possibly

74 appears as the canonical example of transition from a dynamical gene expression regime

75 to a static functional one.

76 Two broad scenarios have been proposed to model this process (see Figure 1). In the

77 first scenario, the period of the individual oscillators is diverging to infinity as they become

78 more anterior (or similarly, the frequency of the clock is going to 0), automatically giving

79 rise to a fixed pattern (Figure 1B-F). This model corresponds to Julian Lewis' model for

80 somitogenesis (appendix of (Palmeirim et al., 1997)), and it is possible to experimentally

81 quantify the period divergence within this model (Giudicelli et al., 2007). This also

82 corresponds to the implicit scenario of many theoretical models assuming that the

83 frequency of the clock goes to 0 as cells get more anterior, such as the models in (Ares

84 et al., 2012; Morelli & Jülicher, 2007), possibly with a sharp discontinuity suppressing

85 period divergence (Jörg et al., 2015). Those models are appealing owing to their simplicity,

86 since all behaviour is encoded in a dynamical frequency gradient (possibly mediated by

87 FGF (Dubrulle & Pourquié, 2004)). However it is unclear what happens from a dynamical

88 systems theory standpoint (a noteworthy exception being the proposal that the gradient

89 emerges through a singularity in phase similar to the Burger's equation (Murray et al.,

90 2013)). In particular, the pattern in this scenario literally corresponds to a frozen clock,

91 such that there is an infinite number of local steady states corresponding to the frozen

92 phases of the oscillators.

93 A second scenario grounded in dynamical systems theory has been proposed (François

94 & Siggia, 2012). In this scenario, a genetic network transits from an oscillatory state to an

5

95   ensemble of (stable) epigenetic states (in Waddington's sense) fixing the pattern.

96   Possible examples include the initial reaction-diffusion based model by Meinhardt

97   (Meinhardt, 1986), or the cell-autonomous model under morphogen control evolved in

98   (François et al., 2007) (Figure 1G). Based on geometric arguments, if bifurcations are

99   local, the most generic model of this transition is expected to present two steps as

100   explained in (François & Siggia, 2012). As a steep control parameter (possibly controlled

101   by a morphogen such as FGF) decreases, the oscillation dies out through a Hopf

102   bifurcation, leading to a single transient intermediate state. Then, for even lower values

103   of the morphogen, one or several new (stable) states appear (technically through saddle-

104   node bifurcations, see Figure 1–figure supplement 1). If the system translates rapidly

105   enough from the oscillatory regime to the multistable regime, a pattern can be fixed

106   (Figure 1H-K). Contrary to the previous scenario where the period of the clock goes to

107   infinity, a Hopf bifurcation is associated to a finite period when the clock stops. The pattern

108   of gene expression itself is laid thanks to multiple expression states discretizing the phase

109   of the clock (Figure 1—figure supplement 1). Importantly, a finite number of states are

110   observed, e.g. anterior and posterior fates within one somite (as first pointed out by

111   Meinhardt (Meinhardt, 1982)).

112   In this paper, we revisit those ideas with explicit modelling to characterize the behaviour

113   of systems transitioning from a dynamical regime (such as an oscillation) to a static

114   multistable regime. We introduce two new assumptions: 1. the two different phases of

115   developmental expression (dynamic and static) can be separated into two independent

116   sets of transcriptional modules acting on several genes simultaneously, and 2. the system

117   smoothly switches from one set to the other. This proposal is motivated by the recent

118   suggestion in insects that different sets of enhancers control waves of gap genes at

119   different phases of embryonic growth (El-Sherif & Levine, 2016). Such assumptions

120   simply explain the so-called "speed-gradient" model in Tribolium (Zhu et al., 2017) (see

121   Figure 1—figure supplement 2). Using both gene network and geometric formalisms, we

122   characterize the types of bifurcations found in systems transitioning from a dynamical to

123   a static regime. We find that surprisingly, if the transition is smooth enough, global

124   bifurcations appear. This situation is different from the standard scenario (Hopf and

125   saddle-nodes) that we nevertheless recover if the transition is more non-linear. This is a

126   generic result that is better studied and understood using geometric models. We further

127   show that the transition through a global bifurcation is more robust than the sequence of

128   Hopf and saddle-node bifurcations with respect to several perturbations that we simulate.

129   Finally, we find that this model can explain many features of metazoan segmentation,

130   such as "speed-gradient" mechanisms or changes of spatial wave profiles due to

131   relaxation-like oscillations. This geometric approach thus offers a plausible scenario

132   underlying embryonic patterning with many associated experimental signatures.

Model

134 In the following, we consider a class of developmental models based on the combination

135 of (at least) two different transcriptional modules. Biologically, those two modules

136 correspond to two sequential developmental phases. The main assumptions are that

137 those transcriptional modules are globally regulated for multiple genes at the same time

138 (which could be done for instance through chromatin global regulations) and that there is

139 a continuous transition from one to the other. Here we focus on metazoan segmentation,

140 notably stabilization of vertebrate segmentation clock or gap gene waves into a striped

141 pattern of genetic expressions, but the formalism might be applicable to other patterning

142 processes where different enhancers with distinct developmental roles have been

143 described.

144 We use ordinary differential equations to model our system. Calling P a vector encoding

145 the state of all proteins in any given cell (typically P corresponds to concentrations of

146 proteins), a generic single-cell equation describing all models presented in the following

147 is:

148
$$\dot{P} = \theta_D(g)\, D(P) + \theta_S(g)\, S(P) + C(P) + \eta(g, P) \qquad (1)$$

149 In Eq. 1, variable g encodes an external control parameter of the developmental transition.

150 For example, g could be an external morphogen concentration driving patterning, but

151 more complex situations with feedback are possible, where g could also be part of the

152 system (e.g. the phase difference between oscillators (Beaupeux & François, 2016;

153 Sonnen et al., 2018)). For simplicity, we rescale variables so that g is constrained

154 between 0 and 1. The terms $D(P)$ and $S(P)$ correspond to different sets of modules, their

8

155 influence on the dynamics being weighted by functions $\theta_D(g)$ and $\theta_S(g)$, respectively.

156 The term $\eta(g, P)$ encodes the noise. Finally, $C(P)$ represents dynamical terms that are

157 independent of the transcriptional modules, such as protein degradation.

158 We focus here on the simplest two-module case, where $S(P)$ encodes a multistable

159 system (i.e. presenting multiple fixed points at steady state) and $D(P)$ a dynamic system

160 (i.e. oscillatory). In this situation we will assume $\theta_S(0) = 1$, $\theta_S(1) = 0$, $\theta_D(0) = 0$, and

161 $\theta_D(1) = 1$, meaning that for $g = 1$ the network is in a pure dynamic phase, while for $g = 1$

162 0 the network is multistable. Details on the specific forms of $D(P)$, $S(P)$, $\theta_D(g)$ and $\theta_S(g)$

163 are given in the following and in the Appendix. We study two types of models: gene-

164 network like models where $D(P)$ and $S(P)$ explicitly model biochemical interactions

165 between genes (such as transcriptional repression), and geometric models where $D(P)$

166 and $S(P)$ directly encode flows in an abstract 2D phase space, similarly to (Corson &

167 Siggia, 2017).

168 We model an embryo as a line of cells, corresponding to the antero-posterior axis. The

169 dynamics within each cell (position x) is described by Eq. 1. The only difference between

170 cells is that the dynamics of g is a prescribed function of x, e.g. we assume that there is

171 a function $g(x, t)$ describing the dynamics of a morphogen. We focus on the transition

172 between the two regimes as g continuously changes from 1 to 0 in different cells as a

173 function of time. We will typically consider a sliding morphogen gradient moving along the

174 antero-posterior axis with speed v, described by $H(s(x - vt))$ where the function H

175 encodes the shape of the morphogen, and parameter s is a measure of the gradient's

176 spatial steepness.

177   We also include noise in the system with the help of an additive Gaussian white noise.

178   For gene networks, we follow an approach similar to the τ-leaping algorithm (Gillespie,

179   2001), where the variance of the noise corresponds to the sum of the production and the

180   degradation terms (approximating independent Poisson noises). A multiplicative noise

181   intensity term $\sqrt{1/\Omega}$ is introduced, where Ω can be interpreted as the typical concentration

182   of the proteins in the system, so that bigger Ω corresponds to lower noise. In addition, we

183   add diffusion coupling the cells in the stochastic gene network models. For the geometric

184   model, the variance of the noise is held independent of the position x. A more detailed

185   description of the noise and diffusion terms is provided in the Appendix.

186   All source codes and data used for this paper are available at :

187   https://github.com/laurentjutrasdube/Dual-

188   Regime_Geometry_for_Embryonic_Patterning

10

Results

A model for the transition between two genetic modules: Hopf vs. SNIC.

In (Zhu et al., 2017), it was suggested that the transition from a "wave-like" behaviour to a static pattern during *Tribolium* segmentation was mediated by a smooth transition from one set of modules (corresponding to the oscillatory phase) towards another one (corresponding to the fixed pattern). This explained the "speed-gradient" mechanism where the typical time-scale of the dynamical system depends strongly on an external gradient (in this case the concentration of *Caudal*). In the Appendix, we further study the associated bifurcation, and observe that new fixed points corresponding to the stabilization of gap gene expressions appear on the dynamical trajectory of those gap genes (Figure 1—figure supplement 2). In simple words, the gap gene expression pattern slowly "freezes" without any clear discontinuity in its behaviour from the dynamic to the static phase, which is reminiscent of the "infinite-period" scenario displayed on Figure 1.

We first aim to generalize this observed property. A simple way to generate many waves of genetic expressions (as in the gap-gene system described above) is to consider an oscillatory process, so that each wave of the oscillation corresponds to a wave of gap genes. We are not saying here that the gap-gene system is an oscillator, but rather that its dynamics can be encompassed into a bigger oscillator (which has actually been suggested as an evolutionary scenario (Verd et al., 2018)). The other advantage of considering oscillators is that we can better leverage dynamical systems theory to identify and study the bifurcations. Furthermore, it allows for a better connection with oscillatory segmentation processes in vertebrates and other arthropods.

11

211   We thus start with an idealized gene regulatory network with 3 genes under the control of

212   two regulatory modules (Figure 2). In the dynamic phase $D(P)$, we assume that the 3

213   genes are oscillating with a repressilator dynamics (Elowitz & Leibler, 2000), so that the

214   system keeps a reference dynamical attractor and an associated period. In the static

215   phase $S(P)$, we assume that the module encodes a tristable system via mutual repression

216   (Figure 2A).

217   We study the dynamics in a simulated embryo under the control of a regressing front of

218   g (Figure 2B). Transition from the dynamic module to the static module is expected to

219   form a pattern by translating the phase of the oscillator into different fates, implementing

220   a clock and wavefront process similar in spirit to the one in (François et al., 2007). We

221   compare two versions of this model, presenting the two different behaviours that we found.

222   In Model 1 (Figure 2C-H), the weights of the two modules are non-linear in g: $\theta_D(g) = g^2$

223   and $\theta_S(g) = (1 - g)^2$ (Figure 2C). In Model 2 (Figure 2I-N), the weights of the two

224   modules are linear in g: $\theta_D(g) = g$ and $\theta_S(g) = 1 - g$ (Figure 2I). We note that the initial

225   and final attractors of both models are identical. Importantly, only the **transition** from one

226   set of modules (and thus one type of dynamics) to the other is different. This two-module

227   system thus offers a convenient way to compare the performance of different modes of

228   developmental transition while keeping the same "boundary conditions" (i.e. the same

229   initial and final attractors).

230   Figure 2E and Figure 2K show the kymographs for both models without noise, with

231   behaviours of individual cells in Figure 2D and Figure 2J. While the final patterns of both

232   models are the same (Figure 2F and Figure 2L), giving rise to a repeated sequence of

233   three different fates, it is visually clear that the pattern formed with Model 2 is more precise

12

234 and sharper along the *entire dynamical trajectory* than the one formed with Model 1, which

235 goes through a "blurry" transitory phase (compare mid-range values of g on Figure 2E

236 and Figure 2K).

237 To better understand this, we plot the bifurcation diagram of both models as a function of

238 g in Figure 2G and Figure 2M. As g decreases, Model 1 is the standard case of a local

239 Hopf bifurcation (Strogatz, 2015) happening at $g = 0.72$. Three simultaneous saddle-

240 node bifurcations appear for lower values of g, corresponding to the appearance of the

241 fixed points defining the three regions of the pattern. The behaviour of Model 2 is very

242 different: the fixed points form on the dynamical trajectory, via three simultaneous Saddle

243 Node on Invariant Cycle (or SNIC) bifurcations. Both models display waves

244 corresponding to the slowing down of the oscillators, leading to a static regime. In Model

245 1, the time-scale disappears with a finite value because of the Hopf bifurcation (Figure

246 2H). For Model 2, it diverges because of the SNIC (Figure 2N), suggesting an explicit

247 mechanism for the infinite-period scenario of Figure 1.

248 To further quantify the differences of performance between the two models, we introduce

249 noise (encoded with variable Ω, see the Model section and the Appendix) and diffusion

250 (Figure 3A-D). We also define a mutual information metric, measuring how precisely the

251 phase of the oscillator is read to form the final pattern (Figure 3E, see the Appendix for

252 details), consistent with the experimental observation in vertebrate segmentation that

253 oscillatory phases and pattern are functionally connected (Oginuma et al., 2010).

254 Intuitively, this metric quantifies in a continuous way the number of fates encoded by the

255 system at steady state. Ideal mutual information for the three mutually exclusive genes of

256 Models 1 and 2 gives $log(3) \sim 1.6$ bits of mutual information, meaning that the pattern

13

257   deterministically encodes the phase of the cycle into three static fates with equal weights.

258   While addition of noise decreases this mutual information as expected (Figure 3E), Model

259   2 (black curves) always outperforms Model 1 (red curves). For a reasonable level of noise

260   corresponding to a few thousands of proteins in the system, Model 2 can encode

261   $2^{1.3} \sim 2.5$ fates, close to the optimum 3. Furthermore, for a given diffusion constant, Model

262   1 requires a ten times smaller noise level than Model 2 to encode the same amount of

263   mutual information, which thus indicates much better noise resistance for Model 2.

264   Those observations suggest that appearance of stable fixed points through SNIC rather

265   than through Hopf generates a more robust pattern. The superiority of Model 2 can be

266   rationalized in the following way: when there is a Hopf bifurcation, only one fixed point

267   exists for a range of g values, so that all trajectories are attracted towards it. This

268   corresponds to the "blurred" zone in the kymographs of Figure 2 and Figure 3. In presence

269   of noise, the effect is to partially erase the memory of the phase of the oscillation when

270   only one fixed point is present for the dynamics. Conversely, a SNIC bifurcation directly

271   translates the phase of the oscillation into fixed points, without any erasure of phase

272   memory, ensuring higher information transfer from the dynamic to the static phase, and

273   therefore more precise patterning. We confirmed these results with similar 3-gene models

274   that used Hill functions for the weights θ_D and θ_S (Figure 2—figure supplement 1 and

275   Figure 3—figure supplement 1).

Gene-free models present a similar geometry of transition

Hopf and saddle-node bifurcations are "local" bifurcations: they do not in principle require complex changes of the flow or fine-tuning of the parameters to happen. As such, they are the most standard cases in many natural phenomena and in most theoretical studies. Conversely, SNIC bifurcations are "global" bifurcations (Ermentrout, 2008): they are associated to global changes of the flows and usually require some special symmetries or parameter adjustments to occur (e.g. to ensure that a saddle-node collides with a cycle).

It is therefore a surprise that SNIC bifurcations spontaneously appear in the model considered here. To better understand how this is possible and if this is a generic phenomenon, we follow ideas first proposed by Corson and Siggia (Corson & Siggia, 2012), and consider geometric (or gene-free) systems. We aim to see if: 1. SNIC bifurcations are generically observed, and 2. a model undergoing a SNIC bifurcation is in general more robust to perturbations than a model undergoing a Hopf bifurcation, with initial and final attractors being held fixed. We thus build 2D geometric versions of the system (variables y and z). The dynamic module $D(P)$ is defined by a non-harmonic oscillator on the unit circle, while the static module $S(P)$ is defined by two fixed points, at $y = \pm 1$, $z = 0$ (see Figure 4A, and the Appendix for the equations). Like previously, we build a linear interpolation between the two systems as a function of g and explore the consequence on the bifurcations (Figure 4B-H). Since the flow in the system is 2D, we can also easily visualize it (Figure 4I and Figure 4—movie supplement 1).

In brief, this geometric approach confirms all the observations made on the gene network model of the previous section, and further clarifies the origin of the SNIC bifurcation. Because of the smooth transition between modules, the entire flow in 2D needs to

299 interpolate from a cycle to a bistable situation. When both modules have close to equal

300 weights (around $g = 0.5$), the flow and associated cycle concentrate around two future

301 fixed points. This appears in retrospect as the most natural way to interpolate between

302 the two situations since both types of attractor (stable limit cycle, and multiple stable fixed

303 points) are effectively present at the same time around $g = 0.5$. For this reason, the

304 oscillations are also more similar to relaxation oscillations, rapidly jumping between two

305 values corresponding to the future fixed points. When g is further lowered, the weight of

306 the static module dominates and "tears apart" the cycle, forming two fixed points.

307 This situation is so generic that in fact, to obtain a Hopf bifurcation, we have to

308 mathematically reinforce the fixed point at $y = 0$ for intermediate g. To do so, we add an

309 extra term and use a non-linear combination of the three terms (see Figure 4—figure

310 supplement 1). In this situation, as expected the flow first concentrates on the central

311 fixed point at $y = 0$, before re-emerging in a bistable pattern for lower g (Figure 4—figure

312 supplement 1I and Figure 4—movie supplement 2). As in the previous section, our mutual

313 information metric confirms that the pattern is more precise when the system goes

314 through a SNIC bifurcation rather than through a sequence of Hopf and pitchfork

315 bifurcations (Figure 4—figure supplement 2). This thus suggests that the properties we

316 observe are generic, and that keeping the static and dynamic attractors fixed, patterning

317 is both more generic and more robustly encoded through a SNIC bifurcation than through

318 a Hopf bifurcation, at least in simple low-dimension models.

16

319 **Robustness and asymmetry in the fixed points**

320 A concern with the results of the previous section might be that those mathematical

321 models are in fact fine-tuned and too symmetrical, so that in particular when the transition

322 occurs, both new fixed points appear for the same value of the control parameter.

323 Furthermore, real biological networks have no reasons to be perfectly symmetrical

324 (although evolution itself might select for more symmetrical dynamics if needed). We thus

325 relax our hypotheses to study a system where parameters and trajectories are not

326 symmetrical (Figures 5 and 6).

327 Going back first to the gene network model, we induce an asymmetry between the fixed

328 points by changing thresholds of repression in the static phase (Figure 5A). The

329 bifurcation diagrams of Figure 5B-C indicate that the asymmetry of the fixed points indeed

330 breaks the simultaneity of appearance of all fixed points in both scenarios. We

331 nevertheless notice that for those changes of parameters, all bifurcations still happen in

332 a very narrow range of g for the SNIC model.

333 Asymmetry of the fixed points might therefore destroy the advantage of SNIC vs Hopf by

334 creating a transient zone where one of the fixed points always dominates. We thus

335 perform a comparison between Models 1 and 2 with the same asymmetric static

336 enhancers (Figure 5, see also Figure 5—figure supplements 1 and 2, and the Appendix

337 for details). To compare the two cases, we consider different time-scales of the

338 morphogen gradient. The reasoning is that the slower the decay of g, the more time the

339 system spends in a region of parameter space without all three final fixed points, allowing

340 the system to relax and "lose" phase information. Conversely, a faster decay of g means

17

341   that less time is spent in a region with few fixed points, and therefore the patterns are

342   expected to be more robust.

343   We first decrease the thresholds of repression of gene A by both genes B and C (Figure

344   5A). Results of these simulations are shown in Figure 5: Model 2 with a SNIC bifurcation

345   still outperforms Model 1 with Hopf and saddle-node bifurcations. In particular, it is again

346   visually very clear on kymographs how Model 2 produces a robust and well-defined

347   pattern at any time point of the simulations, while Model 1 gives rise to a much fuzzier

348   pattern before the transition. Model 1 produces a robust static pattern only for a steep

349   gradient (allowing to quickly move through the "fuzzy" phase) and a weak asymmetry in

350   the static module (Figure 5E). It is brittle to any change of the dynamics of g (Figure 5H)

351   or to stronger asymmetry in the static module (Figure 5—figure supplement 1E,H).

352   Conversely, Model 2 is robust to different shapes of the morphogen (Figure 5F,I). Only

353   for a strong asymmetry does the system lose one fixed point (Figure 5—figure

354   supplement 1I), but even in this case transitions through a SNIC bifurcation appear

355   superior to transitions through a Hopf bifurcation.

356   The fragility of the Hopf bifurcation to asymmetries in the parameters can be understood

357   as follows. In the asymmetric versions of Model 1, one of the fixed points of the static

358   term forms during the Hopf bifurcation, way before the two other fixed points form. It is

359   therefore the only attractor available for a large range of g values. However, in Model 2

360   the same asymmetry only favors one of the saddle-nodes for a small range of g values,

361   generating a robust pattern. Again, we can use the mutual information metric defined

362   above to quantify the robustness of the pattern and confirm the superiority of Model 2

363   (Figure 5—figure supplement 2J). We also confirmed these results for the case of random

18

364 modifications of the repression thresholds of all interactions in the static term (Figure 5—

365 figure supplement 2).

366 The asymmetry introduced in Figure 5 changes the shapes of the basins of attraction and

367 the positions of the fixed points. The geometric model allows to change those features

368 independently. The most generic way to introduce asymmetry in the system is to fix the

369 position of the fixed points of the static regime while only changing the positions of the

370 basins of attraction (the reason is that the future fates depend on the position of the

371 separatrix between different regimes (Corson & Siggia, 2012)). To replicate this situation

372 in the 2D gene-free models, we thus move the unstable fixed point of the static term along

373 the y axis. Results of this procedure are shown on Figure 6 and confirm our results on

374 the network-based models: Model 2 bifurcates via a SNIC and is always more robust than

375 Model 1. When we change the positions of the fixed points in the static regime to move

376 them away from the limit cycle (still in an asymmetric way), interestingly both Models 1

377 and 2 now bifurcate via SNICs (Figure 6—figure supplement 1). Furthermore, we see that

378 for Model 1, the amplitude of the limit cycle decreases before the bifurcation, while for

379 Model 2, the amplitude increases.

380 We conclude from all those numerical perturbations that even with asymmetric basins of

381 attraction and asymmetric parameters, transitions based on SNIC bifurcations are both

382 more generic and more robust than the ones based on Hopf bifurcations.

19

SNIC and asymmetric wave patterns

It is then worth studying other properties of systems transitioning from oscillatory to static patterns. As said above, close to the SNIC bifurcation, the time-scale of the system diverges, suggesting an explicit mechanism explaining infinite-period transitions in metazoan segmentation within a dynamical systems framework. We thus compare the behaviour of the wave pattern in this model to a model where such infinite-period behaviour is assumed, namely the model of a collection of coupled oscillators from (Morelli et al., 2009). A kymograph of the spatio-temporal profile of the frequency imposed on the oscillators is shown in Figure 7A, and the dynamics of the resulting pattern formation process is shown on the kymograph of Figure 7B, with the final pattern on Figure 7C. The most striking difference is observed on the shape of the wave pattern as it moves towards the region where the pattern stabilizes. In the infinite-period scenario of (Morelli et al., 2009), the phase profile is by construction symmetric (albeit stretched in the posterior compared to the anterior, see Figure 7D,E). In the SNIC scenario, we see a clear asymmetry in the wave pattern: the transition from low to high values is sharp, while the transition from high to low values is smooth (Figure 7F, see also Figure 7—movie supplement 1 comparing different scenarios). This phenomenon is observed in all our versions of Model 2 (and is notably absent from all our versions of Model 1, see Figure 7—figure supplement 1). Such asymmetries in the wave pattern are actually observed in somitogenesis, where there is a clear asymmetry in the behaviour of oscillations in the transition within one somite (i.e. anterior to posterior in one somite) vs the transition from one somite to the other (i.e. posterior of one somite to anterior of the next) (Shih et al., 2015). This suggests that our model could offer a simple explanation of wave symmetry,

20

406   solving the long-standing problem of the asymmetry of AP vs PA transitions, which is

407   possibly crucial for segment polarity as first suggested by Meinhardt (Meinhardt, 1982).

Discussion

In this work, we have explored the dynamical properties of generic two-module systems, where one set of modules corresponds to a dynamic phase of genetic expression and the other corresponds to a static phase controlling embryonic patterning. The surprising and unexpected result is that those models typically present global bifurcations where new fixed points appear on the trajectories in phase space (SNIC). SNIC bifurcations come from the smooth interpolation between a flow defining an oscillator in phase space and a landscape characterized by several fixed points. The oscillating attractor then gets continuously deformed until it breaks into several fixed points, leading to the SNIC. This interpolation is a direct consequence of the assumed two-module control as shown on multiple examples above. Importantly, the overall developmental sequence in this context is emergent, since the dynamic close to the bifurcation cannot be understood independently from the static or dynamic modules only. SNIC bifurcations also provide robustness to various perturbations (since, fixed points appearing on cycles better preserve information on the oscillatory phase).

The most straightforward prediction of the model proposed here is the presence of several global transcriptional modules between strongly interacting genes, directly controlling the smooth changes of developmental time-scale (in a similar way to the "speed-gradient" model in (Zhu et al., 2017)). Many developmental genes are regulated by multiple "shadow" enhancers (Cannavò et al., 2016). A smooth transition between different enhancers has even been observed for gap genes in *Drosophila* (El-Sherif & Levine, 2016). Global regulation of transcriptional modules could be biologically achieved through "super enhancers" regulating many genes at the same time (Hnisz et al., 2017). A non-

22

431   trivial prediction of our model is that the intrinsic time-scale of the system is a function of

432   the relative balance of transcriptional activities of the modules. The transcriptional control

433   described here naturally allows for infinite-period bifurcations, an implicit mechanism in

434   several models of metazoan segmentation. This is to be contrasted with classical models

435   of negative feedback oscillators such as the Goodwin model, where the time-scale is

436   entirely controlled by degradation and is independent from transcription/translation rates

437   (Forger, 2011), and delayed oscillators, where the time-scale is essentially controlled by

438   transcriptional delays (Lewis, 2003).

439   Our model is controlled by an external parameter g. The natural hypothesis would be that

440   g corresponds to an actual morphogen gradient, such as *Caudal* in *Tribolium* (Zhu et al.,

441   2017). However, in the spirit of the initial wavefront proposal by Cooke and Zeeman, g

442   could also be in some context a temporal variable, e.g. an effective timer. Recent works

443   on somitogenesis have suggested that the segmentation front could also be coupled to

444   the slowing down of oscillators (Lauschke et al., 2013), so that the oscillation could

445   feedback on itself to define g. It is important to point out that in our framework the nature

446   of the bifurcation does not depend on the nature of g, so it might be difficult to

447   experimentally disentangle feedbacks between the bifurcations and the control parameter

448   from actual properties of the bifurcations themselves. However, irrespective of the nature

449   of g, period divergence would be observed close to the SNIC (and would not be observed

450   for a Hopf bifurcation). We notice though that infinite-period scenarios could be difficult to

451   distinguish from a Hopf bifurcation scenario (with a non negligible frequency change) by

452   simple monitoring of oscillations : for instance, peak-to-peak measurements of the period

23

453   do not show a clear difference between Models 1 and 2 (see Figure 2—figure supplement

454   2).

455   Since the SNIC bifurcations are the generic scenario that we observe in our framework,

456   the mechanism of patterning itself remains largely robust to parameter modifications. This

457   could explain how and why there is so much quantitative variability in segmentation

458   mechanisms such as short/intermediate germ band segmentation (as suggested in (Zhu

459   et al., 2017)), or somitogenesis (number of waves, rescaled period (Gomez et al., 2008)),

460   while the qualitative dynamics itself appears very conserved (see e.g. (Krol et al., 2011)

461   for somitogenesis). In other words, having a two-module mechanism makes the dynamics

462   both more robust – a generic bifurcation scenario gives precise phase encoding – and

463   more evolvable – one can vary many features of the system (e.g. basins of attractions,

464   dynamics of g) and still get proper patterning.

465   The dynamics in this model is smooth, with the same genes interacting to control the

466   system in *both* the dynamic and static regimes. This is consistent with what is observed

467   for gap genes dynamics in short germ insects (Zhu et al., 2017). For vertebrate

468   segmentation, we do not know yet mechanistically how both regimes are controlled, but

469   the Notch signalling pathway is known to gate information from the oscillatory to the

470   segmented regime (Oginuma et al., 2010). An opposite view would be that the transition

471   from dynamic to static regime is *de facto* sudden (even if it appears as smooth for other

472   reasons). Such scenario could be realized in different ways. For instance, different

473   enhancers could regulate completely different sets of genes in the dynamic vs static

474   phases. The "static" genes would then interact with the "dynamic" genes only briefly

475   during development, ensuring transmission of positional information between the static

24

476   and dynamic regions in a very localized region in time and space. In somitogenesis,

477   specific genes are indeed expressed at the so-called "front" (such as Mesp2 (Koseki et

478   al., 2000)) and could act like gating processes transferring the information from the clock

479   to an independent patterning system. In this case, we would be back to a sequential point

480   of view where different regimes of development live in different regions of phase space,

481   and the local bifurcation scenario would then be more plausible (and in fact has appeared

482   in simulations of the evolution of patterning (François et al., 2007)). The problem with this

483   simpler model is that it does not explain *a priori* all other phenomena described here which

484   are direct consequences of the smooth transition from one regime to the other, including

485   period divergence, robustness to changes of morphogen dynamics and to noise.

486   It has been known for a long time that the original Clock and Wavefront model does not

487   require any smooth transition (such as spatial waves of genetic expression) for patterning.

488   But the slowdown of gene expression dynamics during metazoan segmentation appear

489   to be smooth, and the segmentation process itself is experimentally robust to many

490   perturbations, such as changes in morphogen dynamics (Zhu et al., 2017). The model

491   proposed here provides a possible explanation for a smooth robust transition, with a non-

492   trivial (global) bifurcation. Further experimental and theoretical studies are required to

493   assess the importance of smooth transitions for encoding dynamic information into spatial

494   patterns of genetic expressions.

Acknowledgements

We thank members of the François and El-Sherif groups for insightful discussions.

Competing Interests

The authors declare that no competing interests exist.

References

Ares, S., Morelli, L. G., Jörg, D. J., Oates, A. C., & Jülicher, F. F. (2012). Collective modes of coupled phase oscillators with delayed coupling. *Physical Review Letters*, *108*(20), 204101.

Beaupeux, M., & François, P. (2016). Positional information from oscillatory phase shifts : insights from in silico evolution. *Physical Biology*, *13*(3), 1–14.

Cannavò, E., Khoueiry, P., Garfield, D. A., Geeleher, P., Zichner, T., Gustafson, E. H., Ciglar, L., Korbel, J. O., & Furlong, E. E. M. (2016). Shadow enhancers are pervasive features of developmental regulatory networks. *Current Biology*, *26*(1), 38–51.

Cooke, J., & Zeeman, E. C. (1976). A clock and wavefront model for control of the number of repeated structures during animal morphogenesis. *Journal of Theoretical*

515   *Biology*, *58*(2), 455–476.

516   Corson, F., Couturier, L., Rouault, H., Mazouni, K., & Schweisguth, F. (2017). Self-

517   organized Notch dynamics generate stereotyped sensory organ patterns in

518   Drosophila. *Science, 356*(6337), eaai7407.

519   Corson, F., & Siggia, E. D. (2012). Geometry, epistasis, and developmental patterning.

520   *Proceedings of the National Academy of Sciences*, *109*(15), 5568–5575.

521   Corson, F., & Siggia, E. D. (2017). Gene free methodology for cell fate dynamics during

522   development. *ELife*, *6*, e30743.

523   Dubrulle, J., & Pourquié, O. (2004). fgf8 mRNA decay establishes a gradient that

524   couples axial elongation to patterning in the vertebrate embryo. *Nature*, 419–422.

525   El-Sherif, E., Averof, M., & Brown, S. J. (2012). A segmentation clock operating in

526   blastoderm and germband stages of Tribolium development. *Development*,

527   *139*(23), 4341–4346.

528   El-Sherif, E., & Levine, M. (2016). Shadow enhancers mediate dynamic shifts of gap

529   gene expression in the drosophila embryo. *Current Biology*, *26*(9), 1164–1169.

530   Elowitz, M. B., & Leibler, S. (2000). A synthetic oscillatory network of transcriptional

531   regulators. *Nature*, *403*(6767), 335–338.

532   Ermentrout, B. (2008). Ermentrout-Kopell canonical model. *Scholarpedia, 3*(3), 1398.

533   Forger, D. B. (2011). Signal processing in cellular clocks. *Proceedings of the National*

534   *Academy of Sciences*, *108*(11), 4281–4285.

535   François, P., Hakim, V., & Siggia, E. D. (2007). Deriving structure from evolution:

536   metazoan segmentation. *Molecular Systems Biology*, *3*, 9.

537   François, P., & Siggia, E. D. (2012). Phenotypic models of evolution and development:

27

538   geometry as destiny. *Current Opinion in Genetics & Development*, *22*(6), 627–633.

539   Gillespie, D. T. (2001). Approximate accelerated stochastic simulation of chemically

540   reacting systems. *The Journal of Chemical Physics*, *115*(4), 1716.

541   Giudicelli, François, & Lewis, J. (2004). The vertebrate segmentation clock. *Current*

542   *Opinion in Genetics & Development*, *14*(4), 407–414.

543   Giudicelli, F., Ozbudak, E. M., Wright, G. J., & Lewis, J. (2007). Setting the tempo in

544   development: an investigation of the zebrafish somite clock mechanism. *PLoS*

545   *Biology*, *5*(6), e150.

546   Gomez, C., Ozbudak, E. M., Wunderlich, J., Baumann, D., Lewis, J., & Pourquié, O.

547   (2008). Control of segment number in vertebrate embryos. *Nature*, *454*(7202), 335–

548   339.

549   Graf, T., & Enver, T. (2009). Forcing cells to change lineages. *Nature*, *462*(7273), 587–

550   594.

551   Hnisz, D., Shrinivas, K., Young, R. A., Chakraborty, A. K., & Sharp, P. A. (2017). A

552   phase separation model for transcriptional control. *Cell, 169*(1), 13–23.

553   Huang, S., Guo, Y., May, G., & Enver, T. (2007). Bifurcation dynamics in lineage-

554   commitment in bipotent progenitor cells. *Developmental Biology*, *305*(2), 695–713.

555   Jaeger, J., & Monk, N. (2014). Bioattractors: dynamical systems theory and the

556   evolution of regulatory processes. *The Journal of Physiology*, *592*(11), 2267–2281.

557   Jiang, Y. J., Aerne, B. L., Smithers, L., Haddon, C., Ish-Horowicz, D., & Lewis, J.

558   (2000). Notch signalling and the synchronization of the somite segmentation clock.

559   *Nature*, *408*(6811), 475–479.

560   Jörg, D. J., Morelli, L. G., Soroldoni, D., Oates, A. C., & Jülicher, F. (2015). Continuum

28

561   theory of gene expression waves during vertebrate segmentation. *New Journal of*

562   *Physics, 17*(9), 093042.

563   Koseki, H., Saga, Y., Takahashi, Y., Koizumi, K., Takagi, A., Kitajima, S., & Inoue, T.

564   (2000). Mesp2 initiates somite segmentation through the Notch signalling pathway.

565   *Nature Genetics*, *25*(4), 390–396.

566   Krol, A. J., Roellig, D., Dequéant, M.-L., Tassy, O., Glynn, E., Hattem, G., Mushegian,

567   A., Oates, A. C., & Pourquié, O. (2011). Evolutionary plasticity of segmentation

568   clock networks. *Development*, *138*(13), 2783–2792.

569   Lauschke, V. M., Tsiairis, C. D., François, P., & Aulehla, A. (2013). Scaling of embryonic

570   patterning based on phase-gradient encoding. *Nature*, *493*(7430), 101–105.

571   Lewis, J. (2003). Autoinhibition with transcriptional delay: a simple mechanism for the

572   zebrafish somitogenesis oscillator. *Current Biology*, *13*(16), 1398–1408.

573   Meinhardt, H. (1982). *Models of biological pattern formation*. New York, NY: Academic

574   Press.

575   Meinhardt, H. (1986). Models of segmentation. In *Somites in developing embryos* (pp.

576   179–189). Boston, MA: Springer.

577   Morelli, L. G., Ares, S., Herrgen, L., Schröter, C., Jülicher, F. F., & Oates, A. C. (2009).

578   Delayed coupling theory of vertebrate segmentation. *HFSP Journal*, *3*(1), 55–66.

579   Morelli, L. G., & Jülicher, F. F. (2007). Precision of genetic oscillators and clocks.

580   *Physical Review Letters*, *98*(22), 228101.

581   Murray, P. J., Maini, P. K., & Baker, R. E. (2013). Modelling Delta-Notch perturbations

582   during zebrafish somitogenesis. *Developmental Biology*, *373*(2), 407–421.

583   Oginuma, M., Takahashi, Y., Kitajima, S., Kiso, M., Kanno, J., Kimura, A., & Saga, Y.

584   (2010). The oscillation of Notch activation, but not its boundary, is required for

585   somite border formation and rostral-caudal patterning within a somite.

586   *Development*, *137*(9), 1515–1522.

587   Palmeirim, I., Henrique, D., Ish-Horowicz, D., & Pourquié, O. (1997). Avian hairy gene

588   expression identifies a molecular clock linked to vertebrate segmentation and

589   somitogenesis. *Cell*, *91*(5), 639–648.

590   Poston, T., & Stewart, I. (2012). *Catastrophe theory and its applications*. London: Dover

591   Publications.

592   Pusuluri, S. T., Lang, A. H., Mehta, P., & Castillo, H. E. (2018). Cellular reprogramming

593   dynamics follow a simple 1D reaction coordinate. *Physical Biology*, *15*(1), 16001.

594   Sarrazin, A. F., Peel, A. D., & Averof, M. (2012). A segmentation clock with two-

595   segment periodicity in insects. *Science*, *336*(6079), 338–341.

596   Shih, N. P., François, P., Delaune, E. A., & Amacher, S. L. (2015). Dynamics of the

597   slowing segmentation clock reveal alternating two-segment periodicity.

598   *Development*, *142*(10), 1785–1793.

599   Sonnen, K. F., Lauschke, V. M., Uraji, J., Falk, H. J., Petersen, Y., Funk, M. C.,

600   Beaupeux, M., François, P., Merten, C. A., & Aulehla, A. (2018). Modulation of

601   phase shift between Wnt and Notch signaling oscillations controls mesoderm

602   segmentation. *Cell*, *172*(5), 1079–1090.e12.

603   Strogatz, S. H. (2015). *Nonlinear dynamics and chaos: with applications to physics,*

604   *biology, chemistry, and engineering*. Boca Raton, FL: CRC Press.

605   Verd, B., Clark, E., Wotton, K. R., Janssens, H., Jiménez-Guri, E., Crombach, A., &

606   Jaeger, J. (2018). A damped oscillator imposes temporal order on posterior gap

30

607   gene expression in Drosophila. *PLoS Biology*, *16*(2), e2003174.

608   Waddington, C. H. (1957). *The strategy of the genes*. London: Routledge.

609   Wolpert, L., Smith, J., Jessel, T., Lawrence, P., Robertson, E., & Meyerowitz, E. (2006).

610   *Principles of development*. Oxford University Press.

611   Zhu, X., Rudolf, H., Healey, L., François, P., Brown, S. J., Klingler, M., & El-Sherif, E.

612   (2017). Speed regulation of genetic cascades allows for evolvability in the body

613   plan specification of insects. *Proceedings of the National Academy of Sciences*,

614   *114*(41), E8646–E8655.

615

Figures

Figure 1: Scenarios for segment formation.

(*A*) General phenomenology of segment or somite formation. The white to blue gradient represents the oscillating system (e.g. some Notch signaling pathway gene). The determination front (red vertical line) sweeps the embryo in the posterior direction (red arrow) and translates the periodic expression of a genetic clock into a spatial pattern. (*B-F*) Pattern formation with the infinite-period scenario. (*B*) Period divergence is imposed as control parameter g decreases from 1 to 0. (*C*) Two simulated cells with the same dynamics of g end up with different final values of the phase. (*D-E*) Kymographs showing respectively the dynamics of parameter g used in the simulated embryo and the dynamics of the genetic clock. (*F*) Schematic of the final pattern. (*G-K*) Pattern formation with the Hopf scenario. (*G*) Schematic of the gene regulatory network. (*H*) Depending on the dynamics of g, simulated cells can end up with either a high or a low concentration of protein E. (*I-J*) Kymograph showing respectively the dynamics of parameter g used in the simulated embryo and the dynamics of protein E. (*K*) Schematic of the final pattern. The boundary between two segments ("S_i") is set arbitrarily at the transition from high to low concentrations of protein E.

32
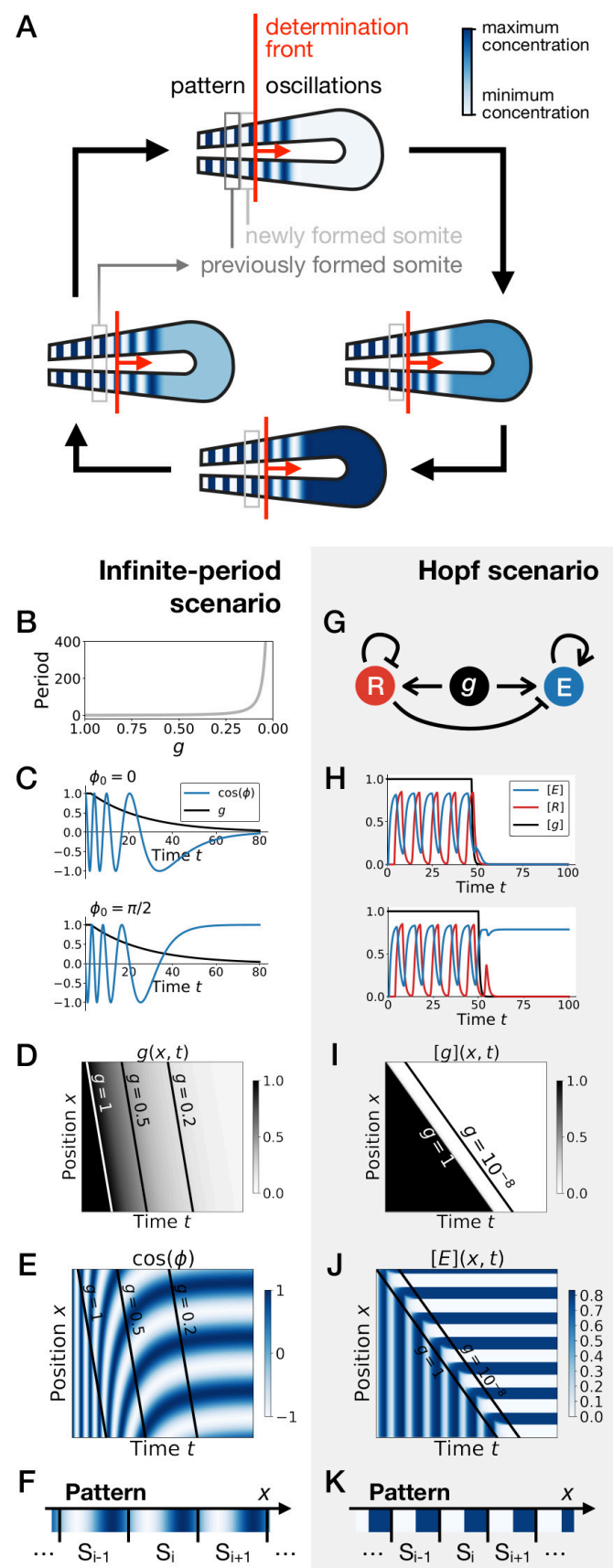
Figure 2: 3-gene models for pattern formation. (*A*) Schematic of the gene regulatory networks encoded by the dynamic term (dotted line) and the static term (solid line). (*B*) Kymograph showing the dynamics of parameter g used in the simulated embryos for both Models 1 and 2. (*C-H*) Simulation results for Model 1. (*C*) Weights of the dynamic (dotted line) and static (solid line) modules as a function of parameter g. (*D*) Gene concentration and value of parameter g inside a representative simulated cell as a function of time. (*E*) Kymograph showing the dynamics of gene expression in the simulated embryo. Transparent colors are used to represent the concentration of the 3 genes, so that mixes of the 3 genes can be easily perceived. Genes *A*, *B*, and *C* are shown in transparent white, blue and purple, respectively. Simulated cells with intermediate concentrations of all genes appear grey. (*F*) Schematic of the final pattern. (*G*) Bifurcation diagram showing the types of dynamics available to the simulated embryo as a function of parameter g. The maximum and minimum concentrations of gene *A* on the stable limit cycles are shown in black. Stable and unstable fixed points are shown in green and red, respectively. "SN" stands for saddle-node bifurcation. (*H*) Period (grey line) and amplitude (red line) of the oscillations along the stable limit cycle. (*I-N*) Simulation results for Model 2.
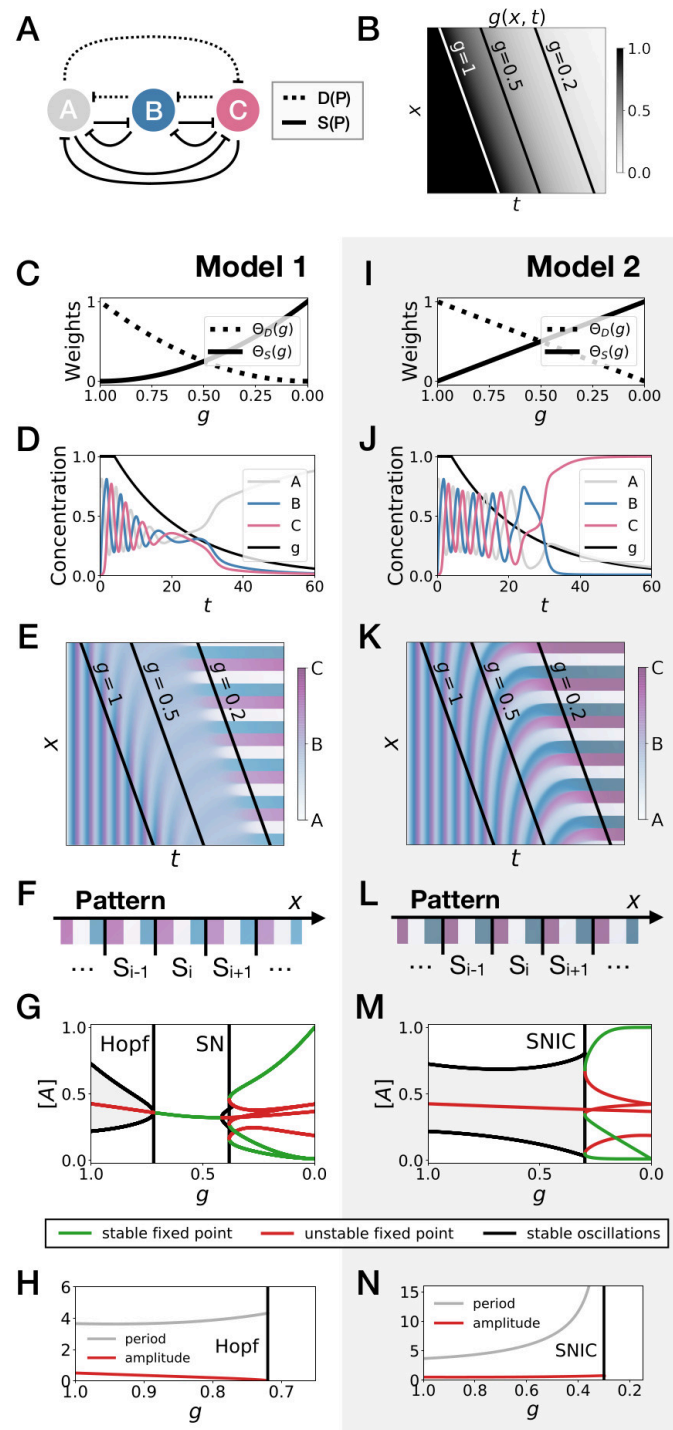
Figure 3: Stochastic simulations of the 3-gene models. (*A-D*) Kymographs showing the stochastic dynamics of gene expression in simulated embryos. The specific values of the typical concentration Ω and of the diffusion constant D used to generate each kymograph are indicated on the panels. The concentration of the three genes at the last simulated time point is shown schematically in the lower part of each panel. (*E*) Mutual information as a function of typical concentration Ω for Model 1 (red lines) and Model 2 (black lines). Paler colors correspond to lower values of the diffusion constant D. The thick horizontal black line indicates the ideal mutual information for 3 mutually exclusive genes. Note that higher values of Ω correspond to lower noise levels.
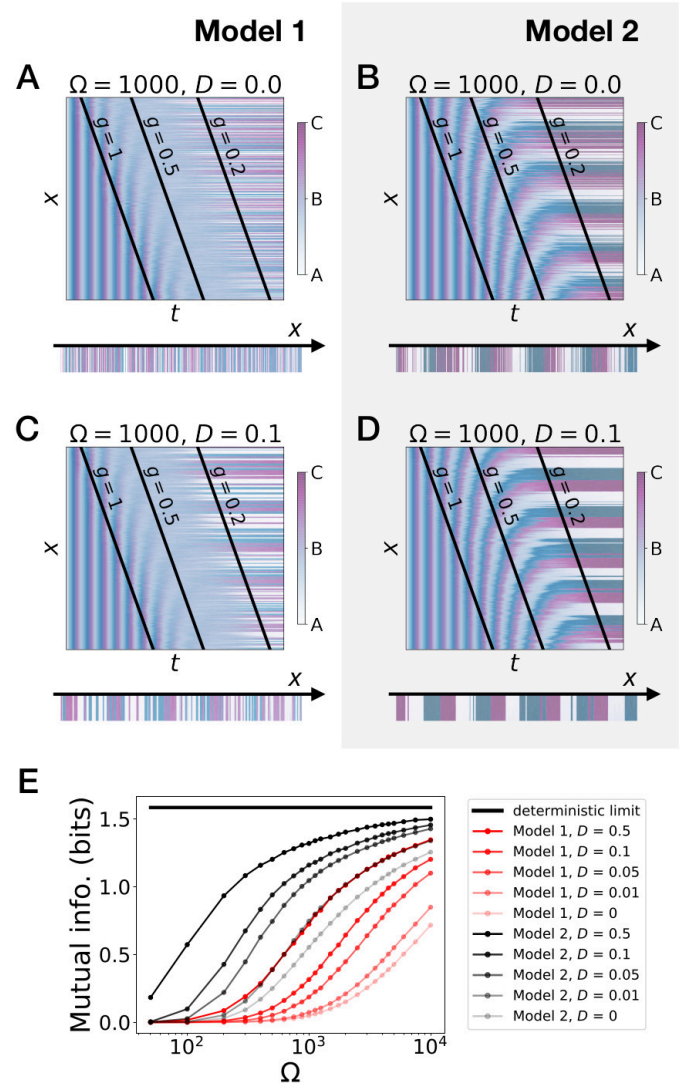
Figure 4: 2D geometric model for pattern formation. (*A*) Schematic of the flow encoded by the dynamic and static terms. The grey circle represents oscillations on the unit circle. Green and red dots represent unstable and stable fixed points, respectively. (*B*) Weights of the dynamic (dotted line) and static (solid line) modules as a function of parameter g. (*C*) Values of geometric coordinates y and z and of parameter g in a simulated cell as a function of time. (*D-E*) Kymographs showing respectively the dynamics of parameter g used in the simulated embryo and the dynamics of coordinate y. (*F*) Schematic of the final pattern. (*G*) Bifurcation diagram showing the types of dynamics available to the simulated embryo as a function of parameter g. The maximum and minimum values of coordinate y on the stable limit cycles are shown in black. Stable and unstable fixed points are shown in green and red, respectively. (*H*) Period (grey line) and amplitude (red line) of the oscillations. (*I*) Flow in phase space for different values of parameter g. The same color scheme than panel *A* is used to represent the cycles and the fixed points. Positions along the limit cycle at time points separated by a fixed time interval are indicated with black dots, so that variations of the speed of the oscillations along the limit cycle can be visualized. The yellow and orange lines represent the y and z nullclines, respectively.

35
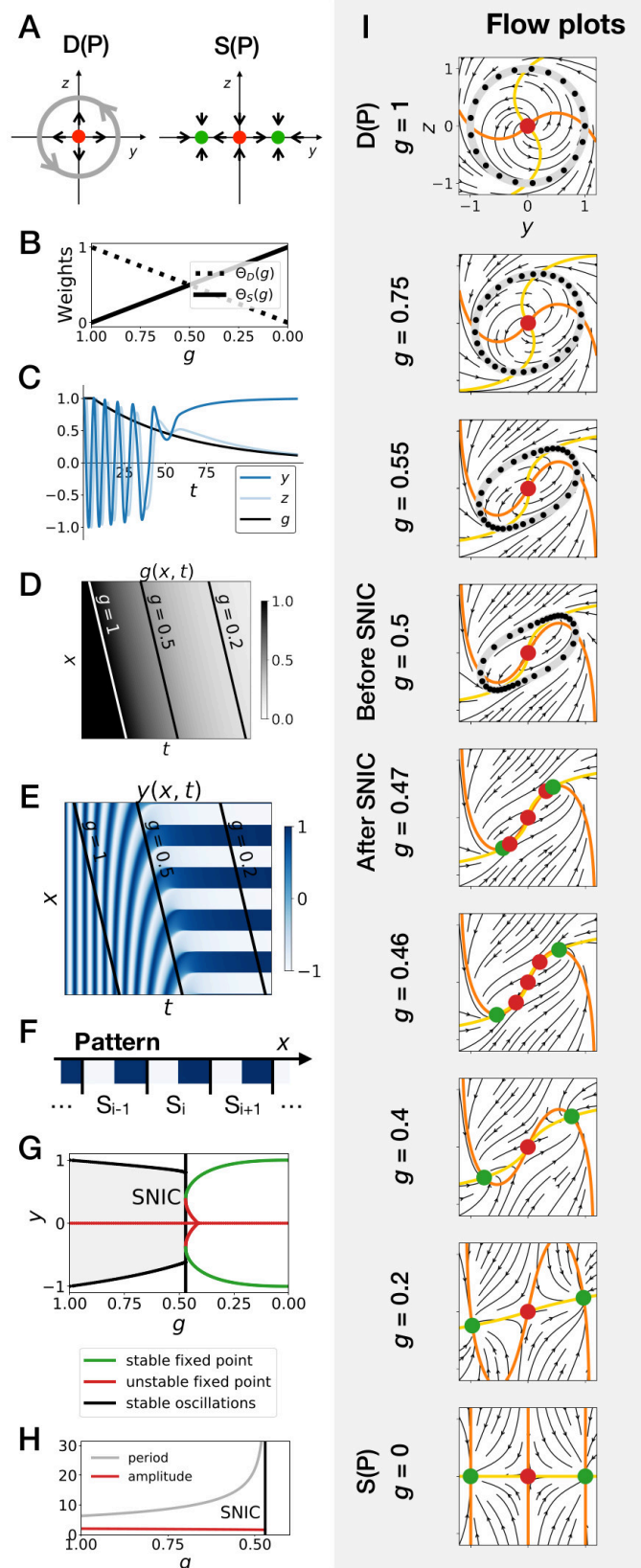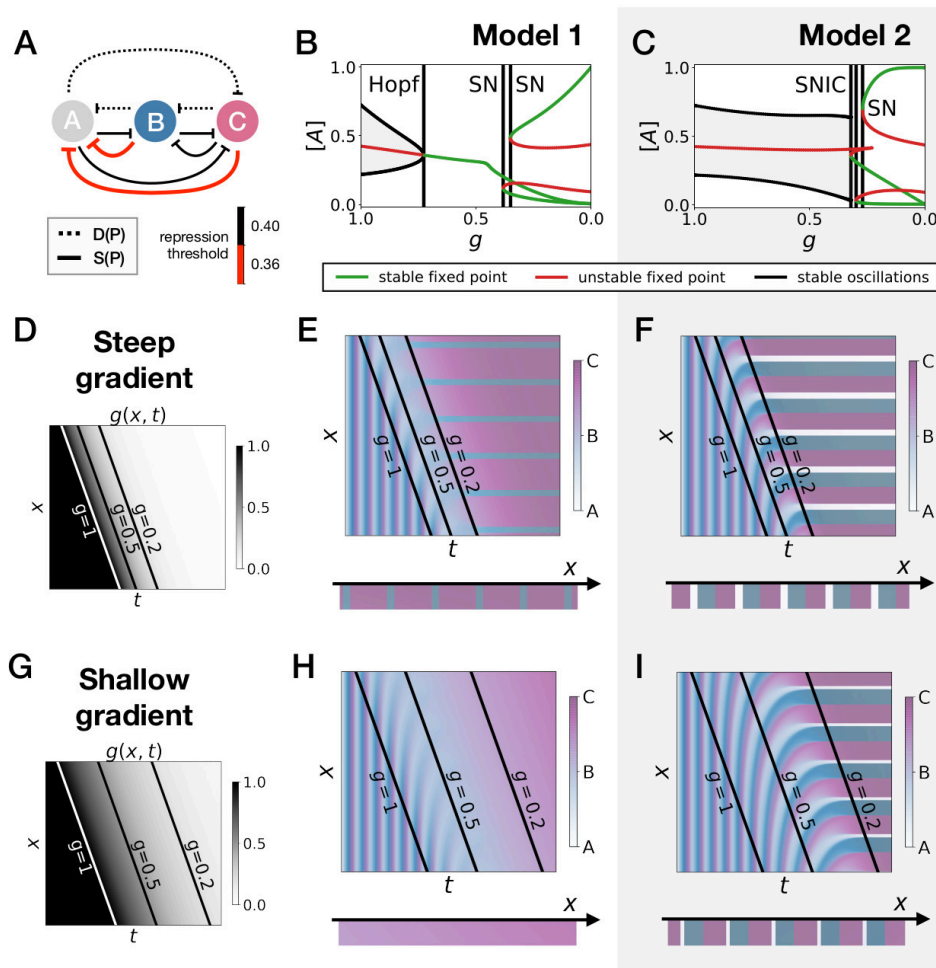
Figure 5: Perturbation of the morphogen gradient steepness in asymmetric 3-gene models. (*A*) Schematic of the gene regulatory networks encoded by the dynamic term (dotted line) and the static term (solid line). The thick red lines indicate stronger repression than the black lines (see the parameters in the Appendix). (*B-C*) Bifurcation diagram showing the types of dynamics available in Models 1 and 2. The maximum and minimum concentrations of gene *A* on the stable limit cycles are shown in black. Stable and unstable fixed points are shown in green and red, respectively. The main bifurcations are identified with vertical lines. "SN" stands for saddle-node bifurcation. (*D-F*) Simulation results for a steep gradient of parameter g. (*D*) Kymograph showing the dynamics of parameter g used in the simulated embryos for both Models 1 and 2. (*E-F*) Kymograph showing the dynamics of gene expression in the simulated embryo of Models 1 and 2. The concentration of the three genes at the last simulated time point is shown schematically in the lower part of the panels. (*H-J*) Simulation results for a shallow gradient of parameter g.

36
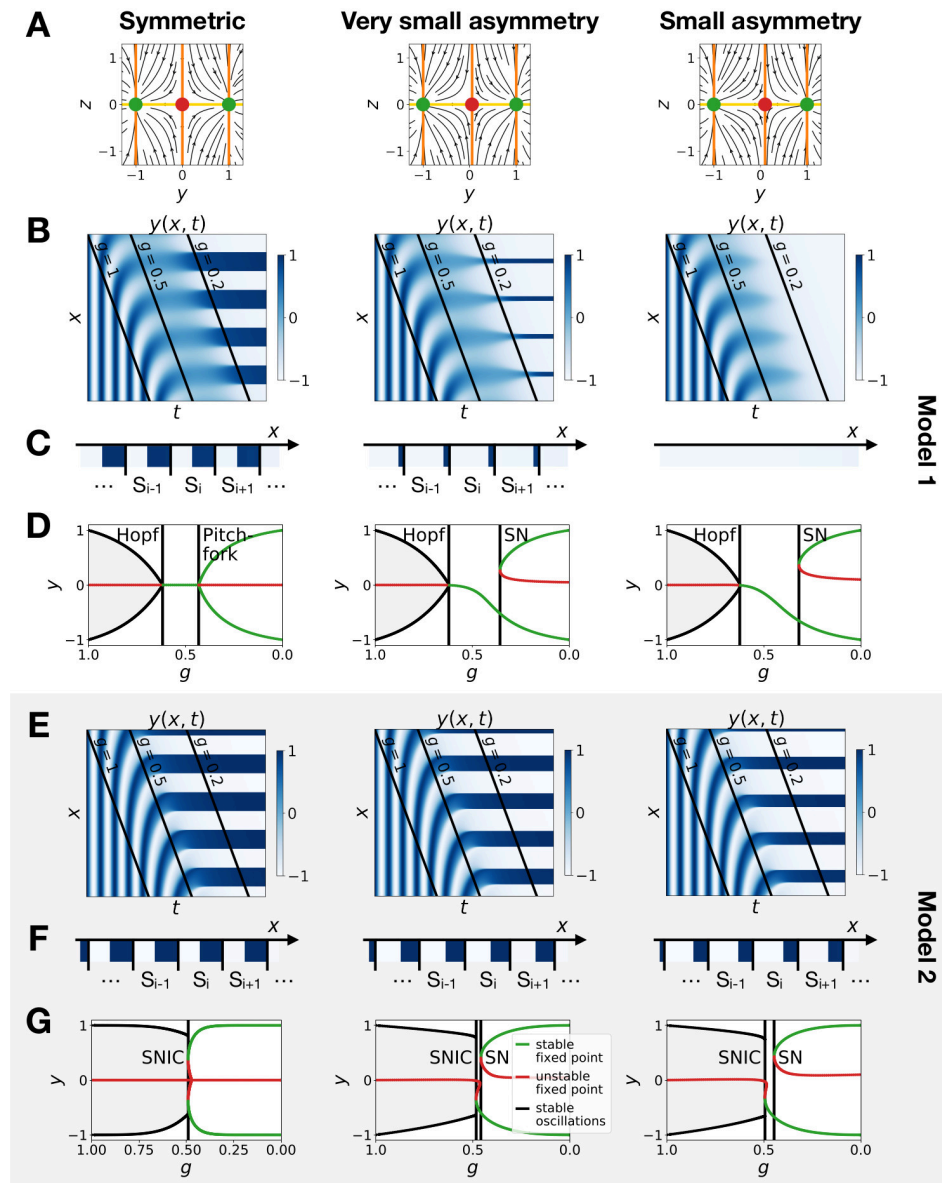
Figure 6: Perturbation of the morphogen gradient steepness in geometric models.

(*A*) Flow plots showing the changes of geometry of the static module. (*B-C*) Corresponding kymographs and final patterns for Model 1. (*D*) Associated bifurcations diagrams. "SN" stands for saddle-node bifurcation. (*E-F*) Corresponding kymographs and final patterns for Model 2. (*G*) Associated bifurcation diagrams.
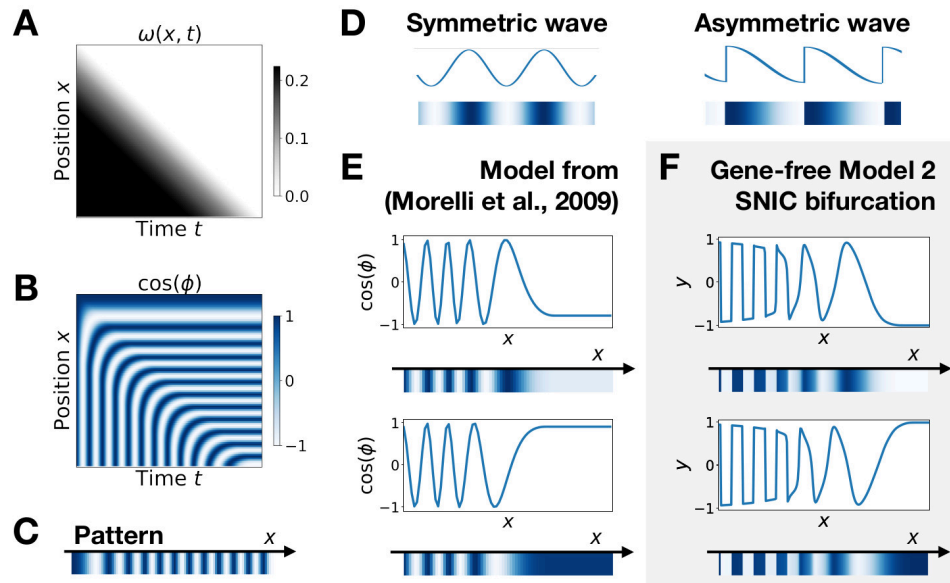
Figure 7: Wave pattern in different models for the infinite-period scenario.
(*A*) Frequency profile for the simulation of the model of coupled oscillators from (Morelli et al., 2009). (*B-C*) Kymograph showing the dynamics of the phase of the oscillators and the corresponding final pattern. (*D*) Two examples of possible wave patterns (symmetrical vs asymmetrical). (*E*) Wave pattern for the model of Panels (*A-C*) for two different time points. (*F*) Wave pattern for Model 2 of Fig. 4 for two different time points.

Supplementary Figures

Figure 1—figure supplement 1: Bifurcation analysis of the Hopf scenario of Fig. 1. (*A*) Bifurcation diagram showing the types of dynamics available to the system as a function of morphogen g concentration. The maximum and minimum concentrations of gene E on the stable limit cycle are shown in black. Stable fixed points are show in green. The main bifurcation events are identified with vertical lines. "SN" stands for saddle-node bifurcation. (*B*) Period of the oscillations along the limit cycle.
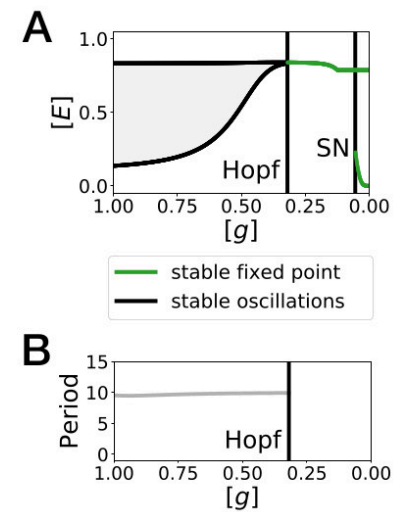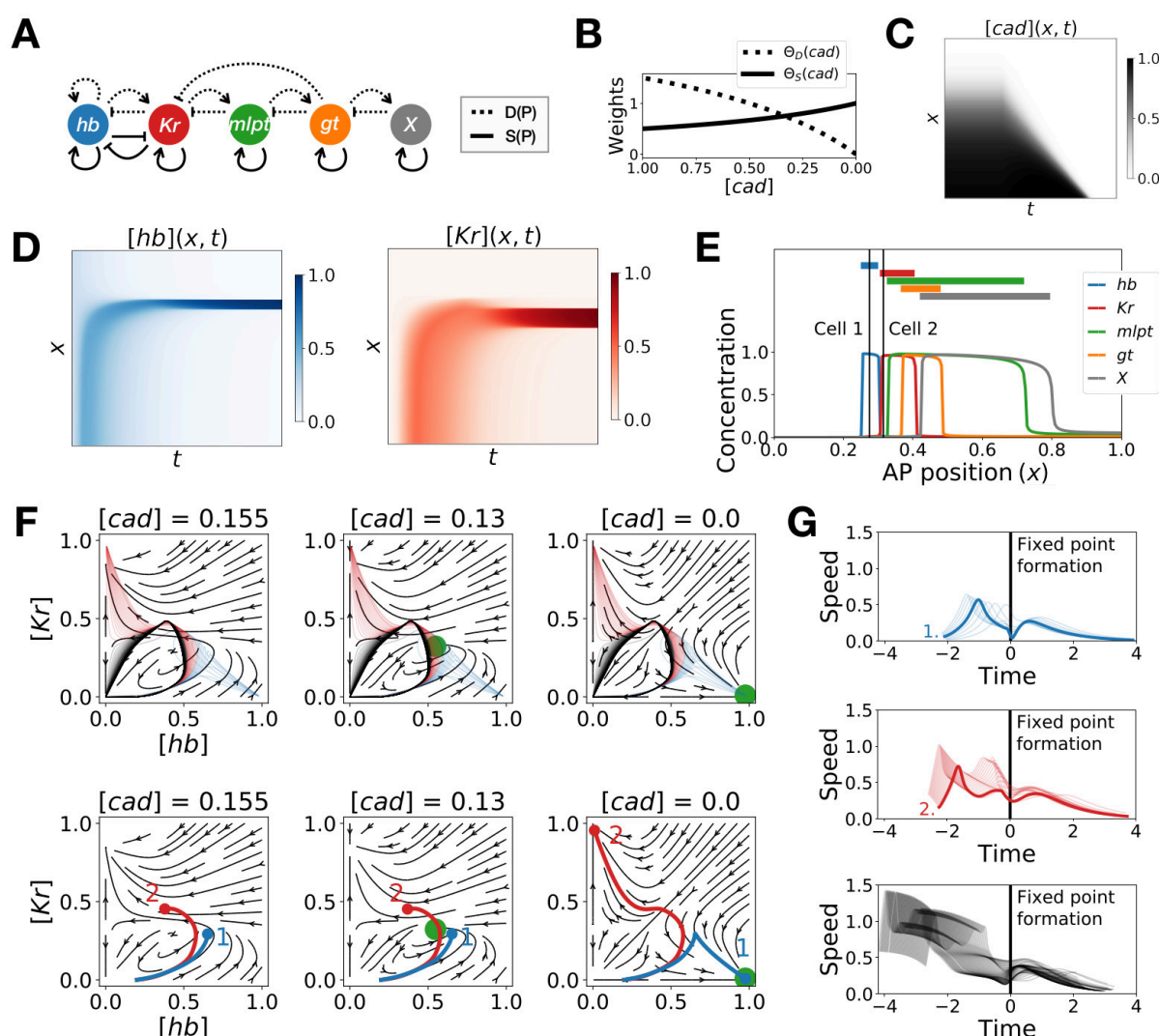
Figure 1—figure supplement 2: Two-enhancer model for Tribolium segmentation.

(*A*) Schematic of the gene regulatory networks encoded by the dynamic term (dotted line) and the static term (solid line). (*B*) Weights of the dynamic (dotted line) and static (solid line) enhancers. (*C*) Kymograph showing the dynamics of the concentration of morphogen *caudal* (*cad*) used in the simulated embryo. (*D*) Kymographs showing the dynamics of the concentration of proteins *hunchback* (*hb*) and *Krüppel* (*Kr*). (*E*) Final pattern of protein expression. The vertical lines identify the positions of the two cells whose trajectories are shown on the bottom subpanels of panel F. (*F*) Flow in the phase space defined by *hb* and *Kr* for different concentrations of morphogen *cad.* The green disk represents the stable fixed point corresponding to the fate with high concentration of *hb*. (*Top subpanels*) Projection of the trajectories of all cells in the *hb-Kr* phase space. The trajectories of cells that end up with high *hb*, *Kr*, and *X* concentrations are represented

40

755   with transparent blue, red and black lines, respectively. (*Bottom subpanels*) Projection of the trajectories of

756   the two cells identified on panel E. For a given cell, the part of the trajectory that is shown is from the initial

757   time point until the time point when *cad* reaches the concentration used to compute the flow. (G) Speed in

758   phase space of all cells as a function of the time since the formation of the fixed point. The top, middle, and

759   bottom subpanels show the speed of the cells that end up with high *hb*, *Kr*, and *X* concentrations at the end

760   of the simulation, respectively. The thick blue and red lines correspond to the speed of cells 1 and 2,

761   respectively.

Figure 2—figure supplement 1: 3-gene models for pattern formation with Hill functions for the weights. (*A*) Schematic of the gene regulatory networks encoded by the dynamic term (dotted line) and the static term (solid line). (*B*) Kymograph showing the dynamics of parameter g used in the simulated embryos for both Models 3 and 4. (*C-H*) Simulation results for Model 3. (*C*) Weights of the dynamic (dotted line) and static (solid line) enhancers as a function of parameter g. (*D*) Gene concentration and value of parameter g inside a representative simulated cell as a function of time. (*E*) Kymograph showing the dynamics of gene expression in the simulated embryo. (*F*) Schematic of the final pattern. (*G*) Bifurcation diagram showing the types of dynamics available to the simulated embryo as a function of parameter g. (*H*) Period (grey line) and amplitude (red line) of the oscillations along the stable limit cycle. (*I-N*) Simulation results for Model 4.
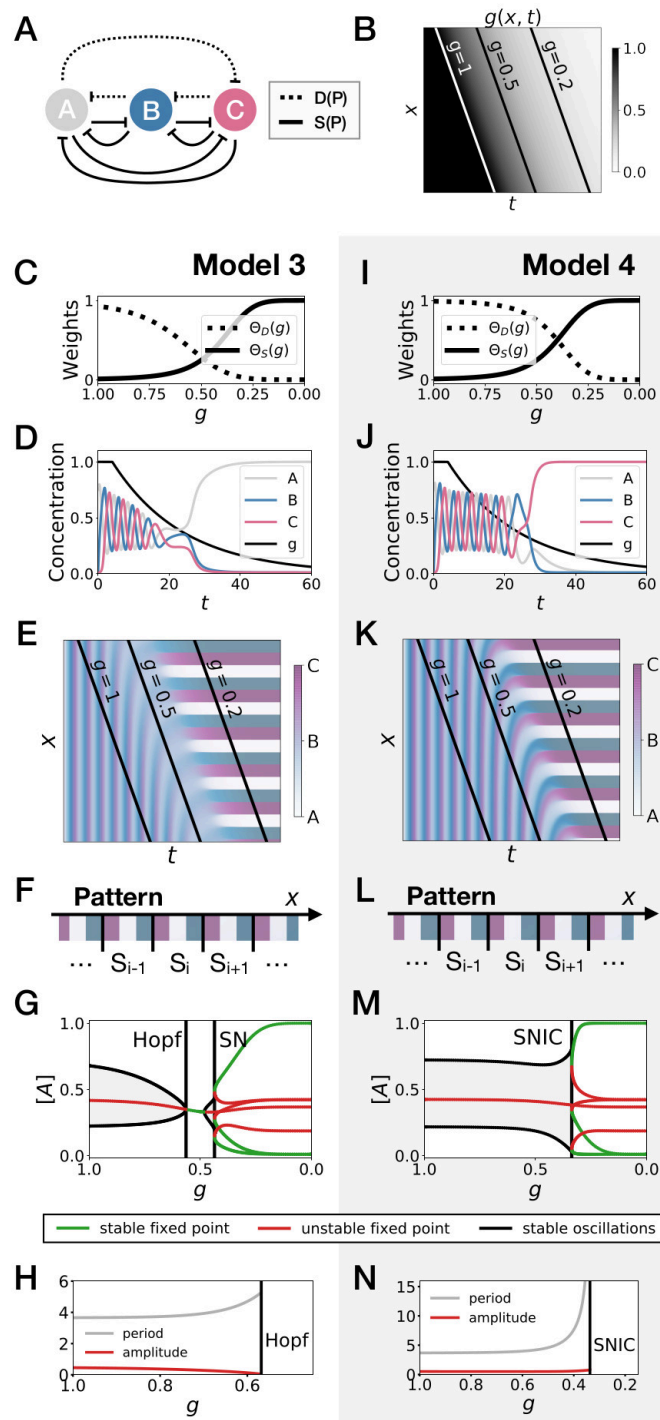
Figure 2—figure supplement 2: Peak-to-peak frequency in the 3-gene models.
The red and black dots represent the normalized peak-to-peak frequency as a function of the position along the antero-posterior (AP) axis for Models 1 and 2, respectively. These data points were computed numerically by using equation 2 of (Giudicelli et al., 2007). The transparent red and black lines are the theoretical normalized frequencies of Models 1 and 2, respectively, obtained via bifurcation analysis. Note that after the Hopf bifurcation in Model 1, the system performs damped oscillations. It is therefore possible to extract a numerical peak-to-peak frequency even after the stable oscillations die during the Hopf bifurcation.

43
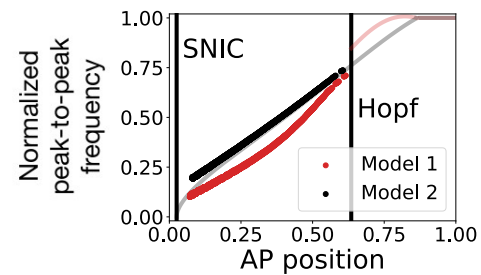
Figure 3—figure supplement 1: Stochastic simulations of the 3-gene models with Hill functions for the weights. (*A-D*) Kymographs showing the stochastic dynamics of gene expression in simulated embryos. The concentration of the three genes at the last simulated time point is shown schematically in the lower part of each panel. (*E*) Mutual information as a function of typical concentration Ω for Model 1 (red lines) and Model 2 (black lines). Paler colors correspond to lower values of the diffusion constant D. The thick horizontal black line indicates the ideal mutual information for three mutually exclusive genes.
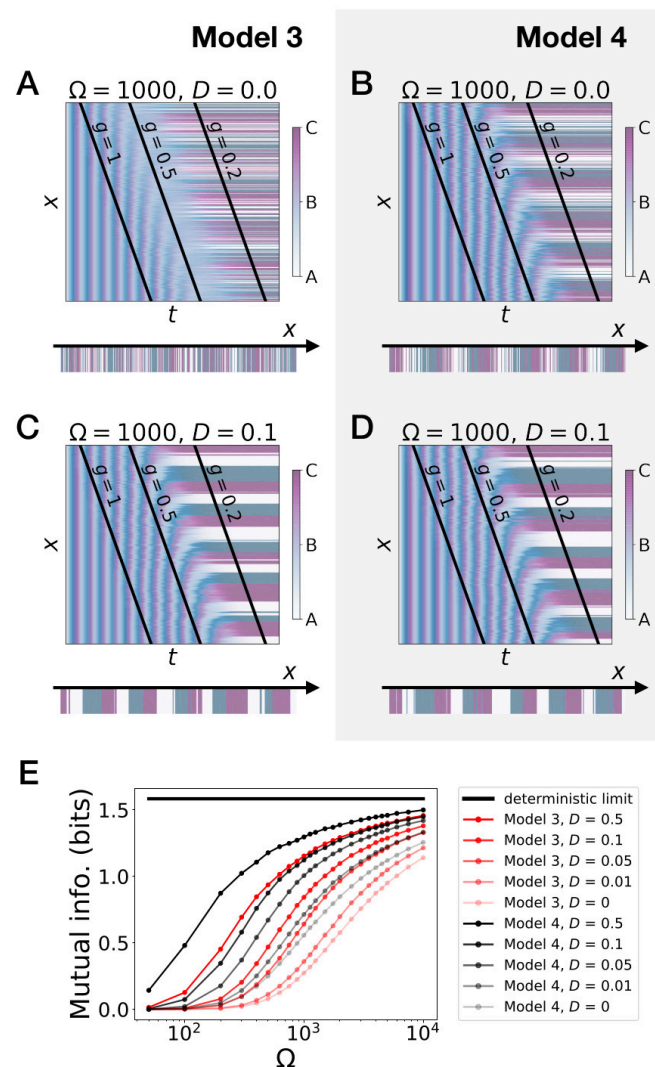
**Figure 4—figure supplement 1: Hopf scenario in the 2D gene-free model.**

(*A*) Schematic of the flow encoded by the dynamic, static and intermediate terms. (*B*) Weights of the dynamic (dotted black line), static (solid black line) and intermediate (solid red line) enhancers as a function of parameter g. (*C*) Values of geometric coordinates y and z, and of parameter g in a simulated cell as a function of time. (*D*) Kymograph showing the dynamics of parameter g used in the simulated embryo. (*E*) Kymograph showing the dynamics of geometric coordinate y. (*F*) Schematic of the final pattern. (*G*) Bifurcation diagram showing the types of dynamics available to the simulated embryo as a function of parameter g. (*H*) Period (grey line) and amplitude (red line) of the oscillations. (*I*) Flow in phase space for different values of parameter g. The limit cycles are represented by thick grey lines. Positions along the limit cycle at time points separated by a fixed time interval are indicated with black dots, such that the (absence of) variations of the speed along the limit cycles can be visualized. The yellow and orange lines represent the y and z nullclines, respectively. The green and red dots represent stable and unstable fixed points, respectively.


45
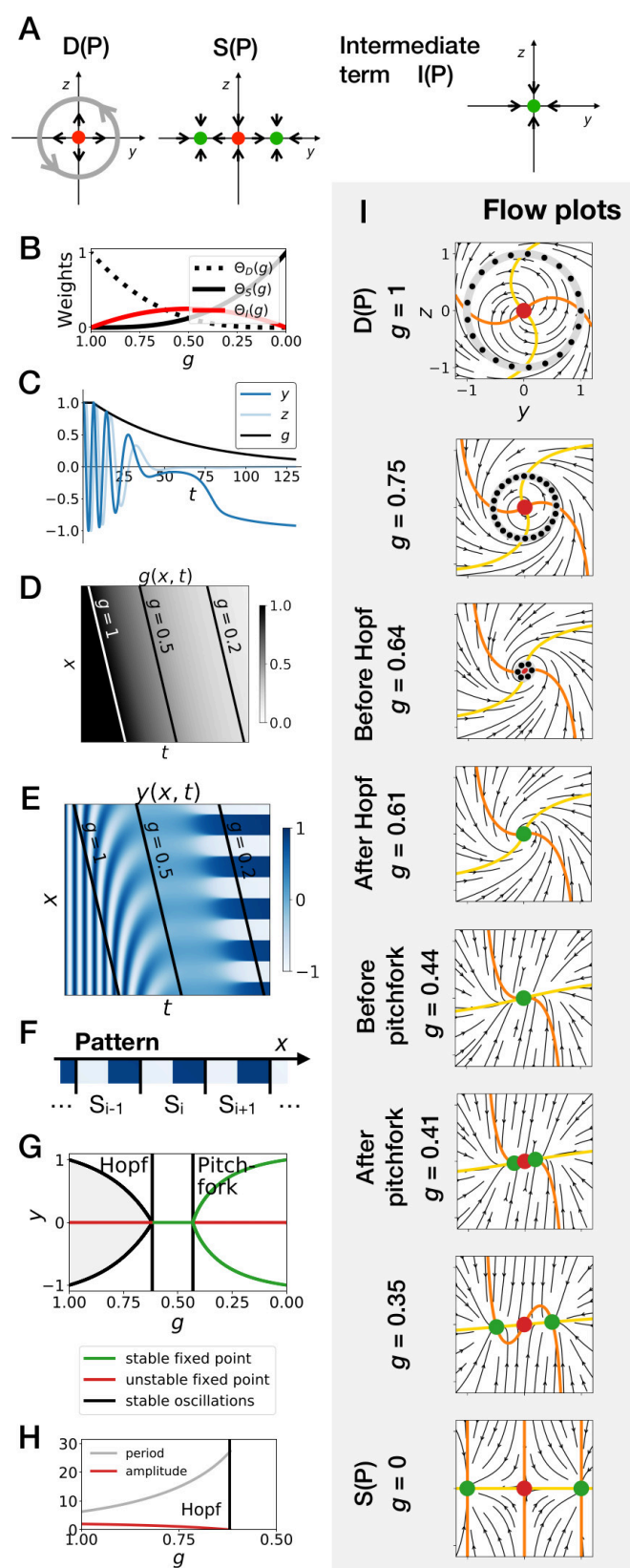
Figure 4—figure supplement 2: Stochastic simulations of the gene-free models.

(*A-B*) Kymographs showing the stochastic dynamics of variable y in simulated embryos. The specific value of parameter Ω used to generate each kymograph is indicated on the panels. (*C*) Mutual information as a function of typical concentration Ω for Model 1 (red line) and Model 2 (black line). The thick horizontal black line indicates the ideal mutual information for a pattern with two symmetric regions.
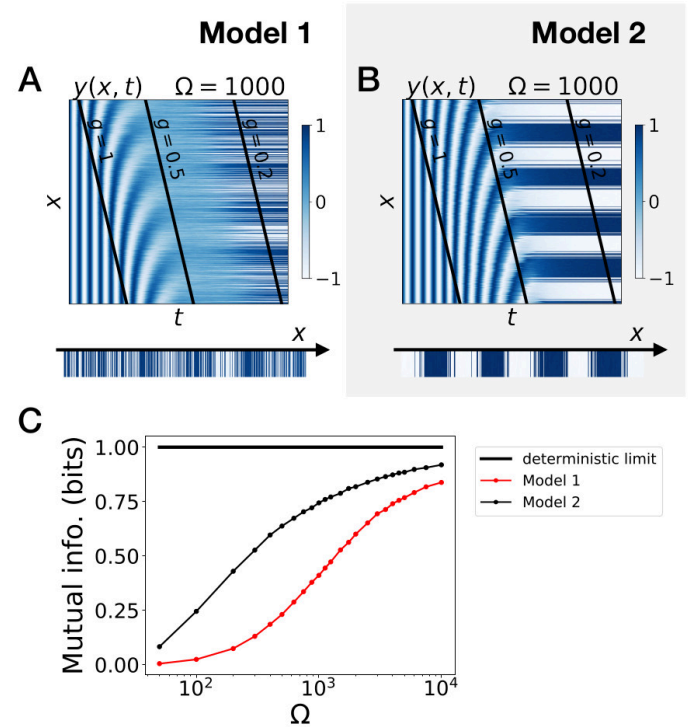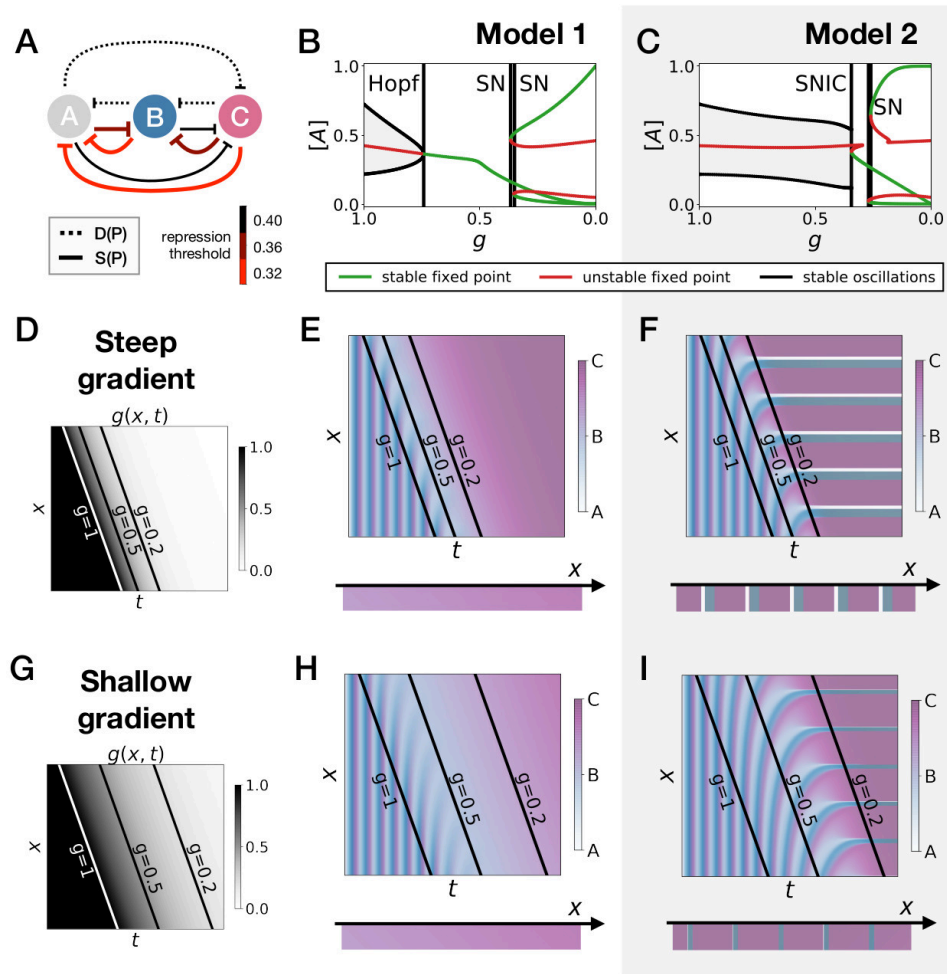
Figure 5—figure supplement 1: Perturbations of the morphogen gradient steepness in strongly asymmetric 3-gene models. (*A*) Schematic of the gene regulatory networks encoded by the dynamic (dotted line) and static (solid line) terms. For each interaction, the color indicates the strength of the repression, with darker shades of red corresponding to weaker repression. (*B-C*) Bifurcation diagram showing the types of dynamics available in Models 1 and 2. "SN" stands for saddle-node bifurcation. (*D-F*) Simulation results for a steep gradient of parameter g. (*D*) Kymograph showing the dynamics of parameter g used in the simulated embryos of both Models 1 and 2. (*E*) Kymograph showing the dynamics of gene expression in the simulated embryos of Model 1. The concentration of the three genes at the last simulated time point is shown schematically in the lower part of the panel. (*F*) Kymograph showing the dynamics of gene expression in the simulated embryos of Model 2. (*G-I*) Simulation results for a shallow gradient of parameter g.

47
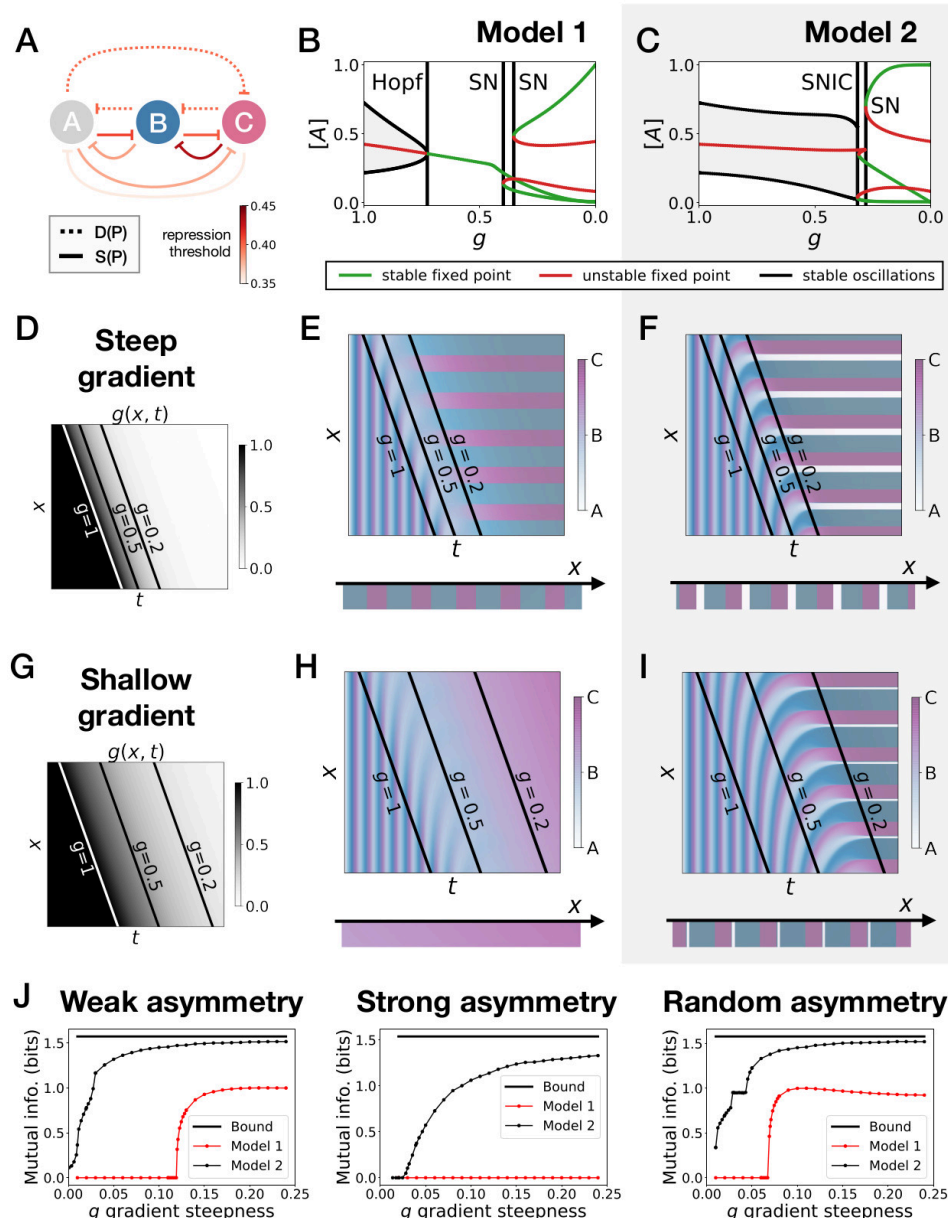
Figure 5—figure supplement 2: Perturbations of the morphogen gradient steepness in randomly asymmetric 3-gene models. (*A*) Schematic of the gene regulatory networks encoded by the dynamic (dotted line) and static (solid line) terms. For each interaction, the color indicates the strength of the repression, with darker shades of red corresponding to weaker repression. (*B-C*) Bifurcation diagram showing the types of dynamics available in Models 1 and 2. "SN" stands for saddle-node bifurcation. (*D-F*) Simulation results for a steep gradient of parameter g. (*D*) Kymograph showing the dynamics of parameter g used in the simulated embryos of both Models 1 and 2. (*E*)

854   Kymograph showing the dynamics of gene expression in the simulated embryos of Model 1. The

855   concentration of the three genes at the last simulated time point is shown schematically in the lower part of

856   the panel. (*F*) Kymograph showing the dynamics of gene expression in the simulated embryos of Model 2.

857   (*G-I*) Simulation results for a shallow gradient of parameter g. (*J*) Mutual information as a function of the

858   steepness of the g gradient for Models 1 (red line) and 2 (black line). The thick horizontal black line indicates

859   the theoretical upper bound. The left, center and right subpanels show respectively the mutual information

860   for models with a weak asymmetry in the fixed points of the static term (Fig. 5), with a strong asymmetry

861   (Supp. Fig. 7) and with a random asymmetry (this figure).
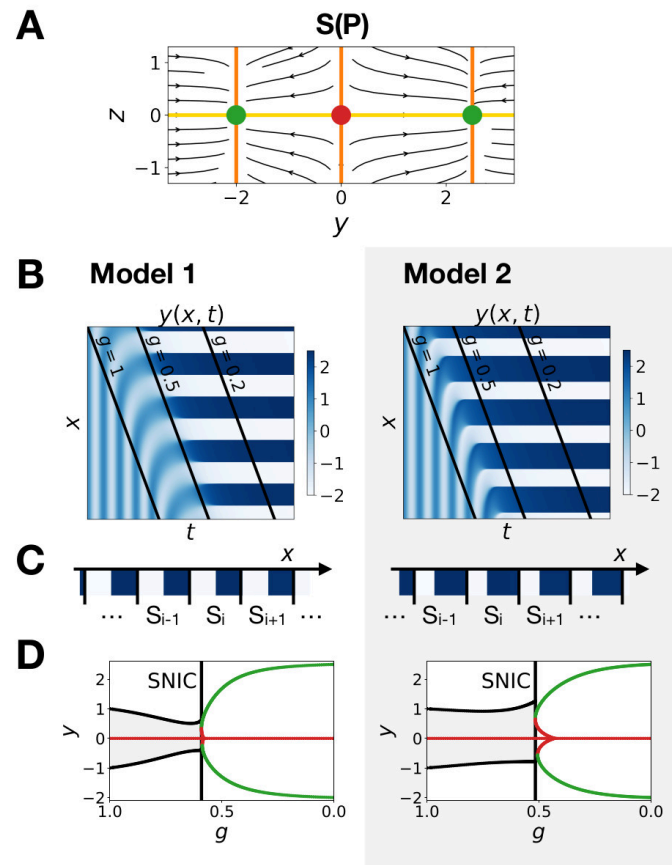
862 **Figure 6—figure supplement 1: Model 1 becomes a SNIC when fixed points are**

863 **outside the limit cycle.** (*A*) Flow plots showing the change of geometry of the static module. (*B-C*)

864 Corresponding kymographs and final patterns for Models 1 and 2. (*D*) Associated bifurcations diagrams.
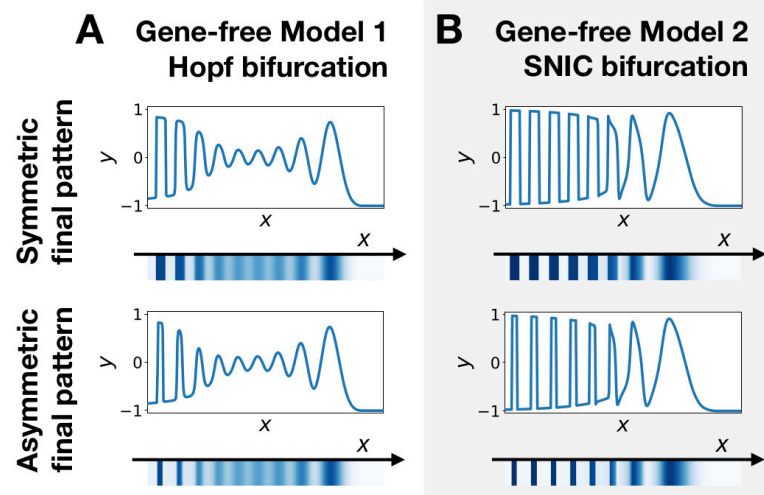
Figure 7—figure supplement 1: Wave pattern in different versions of the 2D gene-free model. (*A*) Wave patterns of the gene-free Model 1 with a Hopf bifurcation. The top and bottom subpanels show the wave pattern for symmetric and asymmetric fixed points in the static term, respectively. (*B*) Wave patterns of the gene-free Model 2 with a SNIC bifurcation.

Supplementary Movie Legends

Figure 4—movie supplement 1: Flow of the gene-free with a SNIC bifurcation. Flow in phase space as parameter g goes from 1 to 0. The limit cycles are represented by thick grey lines. The yellow and orange lines represent the y and z nullclines, respectively. The green and red dots represent stable and unstable fixed points, respectively.

Figure 4—movie supplement 2: Flow of the gene-free with a Hopf bifurcation. Flow in phase space as parameter g goes from 1 to 0. The limit cycles are represented by thick grey lines. The yellow and orange lines represent the y and z nullclines, respectively. The green and red dots represent stable and unstable fixed points, respectively.

Figure 7—movie supplement 1: Comparison of pattern formation dynamics in different models. Dynamics of the spatial wave patterns in four models: a phase model with diverging period similar to the infinite-period scenario of Figure 1, the symmetric gene-free Model 1, the symmetric gene-free Model 2, and the asymmetric gene-free Model 2.